



INTERNATIONAL ATOMIC ENERGY AGENCY  
UNITED NATIONS EDUCATIONAL, SCIENTIFIC AND CULTURAL ORGANIZATION  
**INTERNATIONAL CENTRE FOR THEORETICAL PHYSICS**  
I.C.T.P., P.O. BOX 586, 34100 TRIESTE, ITALY, CABLE: CENTRATOM TRIESTE



H4.SMR/383 - 17

Giuliano BENELLI, Vito CAPPELLINI

Dipartimento di Ingegneria Elettronica, Facoltà di Ingegneria  
Università degli Studi di Firenze, Italia

WORKSHOP ON REMOTE SENSING TECHNIQUES  
WITH APPLICATIONS TO AGRICULTURE, WATER  
AND WEATHER RESOURCES

(27 February - 21 March 1989)

DIGITAL PROCESSING TECHNIQUES OF SAR IMAGES  
FOR REMOTE SENSING APPLICATIONS

DIGITAL PROCESSING TECHNIQUES OF SAR IMAGES  
FOR REMOTE SENSING APPLICATIONS

V. CAPPELLINI  
University of Florence  
and  
IROE - CNR  
Florence  
ITALY

## ABSTRACT

In this paper digital techniques for image processing and automatic classification in remote sensing applications are described. Digital filters, suitable for radar noise reduction, are first described. Some algorithms using the Bayes rule or block distance for the automatic classification and discrimination of agricultural crops are presented. Microwave images, obtained by employing synthetic aperture radars and collected during the European SAR 580 campaign, are used to evaluate the performance of these processing algorithms.

## 1. INTRODUCTION

The use of multispectral scanners from satellite or aircrafts is quite attractive in crop classification by means of remote sensing. Very promising results have been obtained by using the observations in the optical band through multispectral scanners. However, in order to achieve a satisfactory performance, several observations during the crop growth cycle are often necessary. Since these optical observations are strongly affected by weather conditions, the use of radar images can significantly improve the performance of any real method for crop classification. Depending on the frequency and observation angle, radars permit to investigate different vegetation layers and soil surfaces under plants and to increase the information obtained through the optical data.

At present only few investigations have been carried out in radar potential for crop classification and discrimination problems [1,2]. However, also in this case, the contribution of microwave images can be very important.

In this paper, the use of microwave images obtained by using a Synthetic Aperture Radar (SAR) in remote sensing and, particularly, in agricultural applications, is analyzed. SAR images generally require efficient pre-processing operations in order to reduce noise and degradations. In fact, the signal-to-noise ratio in these images is quite low and, therefore, their quality must be enhanced before applying any classification algorithm. However, the standard image pre-processing techniques which are used to enhance non-coherent optically produced images are not suitable for SAR images, due to the coherent nature of the radar imaging process. In this paper, some different spatial digital filters suitable for SAR images, are first analyzed. Some different multidimensional algorithms for the automatic classification and discrimination of agricultural crops are described.

The performance of these classification algorithms is evaluated by using some images collected during the European SAR 580 campaign in June 1981. Microwave SAR images in X and C bands and some images in the infrared region of the test area are available. At the same time, the real data, directly collected through an extensive ground survey, permit to evaluate the probability of correct classification of different crops. The results show that a high performance can be achieved only by using multidimensional classifiers.

## 2. DIGITAL FILTERS FOR SAR IMAGES AND CLASSIFICATION ALGORITHMS

SAR images are generally affected by a multiplicative noise, called fading, which influences the scattering coefficient  $\sigma$ . A radar image  $g(i,j)$  of dimensions  $N \times N$  is obtained by measuring the power reflected by the terrain as a function of the position. Generally, a radar image is comprised of many homogeneous areas, each area belonging to a particular terrain feature. The reflectivity at each point can be modeled as a stationary random process  $r(i,j)$ . The fading, due to the coherent nature of the radar process, introduces a multiplicative noise  $n(i,j)$  in the image; the point spread function  $h(i,j)$  further degrades the quality of the image. Therefore, the available image can be written as:

$$(1) \quad g(i,j) = [r(i,j) \cdot n(i,j)] * h(i,j)$$

where  $*$  denotes the convolution operation. Equation (1) is a model for SAR images, which has been found suitable for digital processing operations.

The noise  $n(i,j)$  is generally modeled as a stationary, white, non-Gaussian random process with a  $\chi^2$  probability density function having  $2m$  degrees of freedom, where  $m$  is the number of independent radar returns that were averaged.

The signal-to-noise ratios in SAR images is often quite low; therefore, a digital filtering operation is required in order to mitigate the effect of the noise. However, digital filters are able to reduce the multiplicative noise. The two more efficient classes of digital filters for SAR images have been proposed by Lee [4] and Frost [5,6].

The Lee and Frost filters present similar characteristics: they operate in the spatial domain, are adaptive filters and are designed by minimizing the mean squared error (MSE). The model used for the radar image is given by equation (1). The term  $h(i,j)$  represents the distortion introduced by the radar system and it is independent of the data. It can be determined through the knowledge of the radar characteristics and can be removed. In order to explain the behaviour of these filters, the image model is assumed as given by:

$$(2) \quad g(i,j) = r(i,j) \cdot n(i,j)$$

In the Lee filter the non-linear model (2) is replaced by an approximated linear model. The approximated estimate  $g'(i,j)$  of the actual pixel is defined as:

$$(3) \quad g'(i,j) = a \cdot r(i,j) + b \cdot n(i,j) + c$$

where  $a$ ,  $b$ , and  $c$  are three constants, defined in such a way as to minimize the MSE error between  $g(i,j)$  and  $g'(i,j)$ . The Lee filter is an adaptive filter, based on the local statistics and computationally efficient, but it tends to blur the boundaries. The Frost filter characteristics of the Frost filter are similar to those of the Lee filter, but it preserves the edge structure.

The impulse response  $m(i,j)$  of the Frost filter that provides an estimate  $g'(i,j)$  of the image is obtained by minimizing the MSE error given by:

$$(4) \quad \xi^2 = E [g'(i,j) - g(i,j) \cdot m(i,j)]^2$$

After some mathematical transformations, it results :

$$(5) \quad m(i,j) = k_1 \beta \exp(-\beta \sqrt{i^2 + j^2})$$

being

$$(6) \quad \beta = k_2 \sigma_g^2 / [\bar{g}(i,j)]^2$$

where  $k_1$  and  $k_2$  are two normalizing constants and  $\sigma_g^2$  is the variance of the real image. Therefore, in order to implement the filter, the two parameters  $g(i,j)$  and  $\sigma_g^2$  must be given. They can be estimated from the real image by considering a small window centered at the actual processed pixel.

The final problem in remote sensing is the interpretation of the data collected through different sensors. Therefore, a classification and discrimination of some terrain or vegetation characteristics contained in the examined area must be generally performed. In order to achieve high performance, it is generally necessary to have many images  $g_1(i,j), g_2(i,j), \dots, g_n(i,j)$  of the same area obtained through different sensors and/or in different bands.

The classification algorithm can be subdivided in two classes : i) the parametric or statistical algorithms and ii) the non-parametric algorithms. The algorithms of the second class are used when the objects in the scene have reasonably distinct signatures. On the other hand, the statistical algorithms assume a particular statistical distribution for each element to be classified and estimate the parameters of this distribution, as mean vector and covariance matrix, to be used in the classification algorithms. The statistical algorithms are particularly suitable for agricultural crops and vegetations.

The most popular statistical algorithm is that using the maximum likelihood or Bayes rule. Let us consider the case in which  $m-1$  different classes of agricultural crops must be classified by using  $n-1$  different images of the same area. In order to explain the Bayes algorithm, the simple case  $n=1$  is first considered. Different crops give rise to different reflected power and, therefore, to different gray levels in the image. A probability density function of the gray levels  $x$  for each crop can be defined. In agricultural applications, this density function can be approximated in many cases through a Gaussian function, with mean and variance depending on the considered crop.

The Bayes classifier operates in the following way : the pixel to be classified has value  $x$ , then it is classified in the class  $i$  if :

$$(7) \quad p(i/x) = \max_{j \neq i} p(j/x)$$

In the case of a Gaussian distribution, the Bayes rule reduces to choose the class  $i$  having the highest  $D_i(x)$  defined as :

$$(8) \quad D_i(x) = \ln p(i) - \frac{1}{2} \ln(\sigma_i^2) - (x - \mu_i)^2 / 2\sigma_i^2$$

where  $\mu_i$  and  $\sigma_i^2$  denote the mean and variance of the class  $i$ .

The Bayes classifier with  $n$  dimensions can be defined in a similar way. In this

case, a pixel is classified by using  $n$  different values  $x = (x_1, x_2, \dots, x_n)$ , which are the gray levels in the  $n$  images. The Bayes algorithm is optimum in terms of the probability of correct classification when all the probability density functions are Gaussian functions. However, it requires high-time computation, particularly for  $n \geq 1$  and high  $m$ .

In many cases, it is suitable to use sub-optimum classification algorithms which are simpler to be implemented. A commonly used method for statistical classification is the minimum distance classifier. In this algorithm, a pixel characterized by the gray levels  $x = (x_1, x_2, \dots, x_n)$  is assigned to the  $i$ -th class having the mean vector  $M_i$  nearest to  $x$ . Different algorithms can be implemented, depending on the distance definition.

The Euclidean classifier uses the Euclidean distance between  $M_i$  and  $x$  defined as :

$$(9) \quad d_1^2(x) = \sum_{j=1}^n (x_j - \mu_{i,j})^2$$

Another measure of distance, called city block distance, is sometimes used in the classification algorithms and is given by :

$$(10) \quad d_1^2(x) = \sum_{j=1}^n |x_j - \mu_{i,j}|$$

### 3. RESULTS

The image and data used in this paper were collected during the European SAR 580 campaign in June 1981. The surveyed area was located in a farm of Southern Tuscany, called Castel di Pietra. The main crops of this typical Mediterranean area are corn, wheat, alfalfa, sunflowers and olive trees. Fig. 1 shows a map of the surveyed area and the crops present in the farm during the flight. About two hours before the flight, a survey with an airborne multispectral scanner was carried out. Many real data were collected through an extensive ground survey in the farm before, during and after the SAR campaign.

Images in X (24-37.5 mm) and C (37.5-75 mm) bands with HH polarization were recorded during the flight. A small area of the SAR images was digitized and used in this paper. The original X and C band images are shown in Figs. 2 and 3, respectively. Other four optical and IR images are also available and have been used to facilitate the classification operation. In particular, the image shown in Fig. 4, which refers to the IR band, will be used in the results presented in this section. As it can be seen from these figures, the signal-to-noise ratio in the SAR image is quite low; therefore, a filtering operation must be applied. Some different classes of digital filters have been proved. However, the more suitable filters are the Lee and the Frost filters. As an example, the image obtained from the original X band of Fig. 2 by applying the Frost filter is shown in Fig. 5. The local mean and variance were computed in both cases by using a window of 5x5 pixels.

The performance of the classification algorithms is evaluated by computing the probability of correct classification of each crop. This probability is evaluated by using the truth data directly collected during the ground survey.

The case of on-dimensional algorithms using only a band (X or C) is first considered. The probability of correct classification by using the Bayes rule is given in Table 1, when a Frost filter is used. Similar results have been obtained by using the band C. Fig. 6 summarizes the results obtained for the two bands and reports the mean probability of correct classification, averaged on the four crops. It can be seen that the Frost filter permits the achievement of a slight improvement with respect to the Lee filter. At the same time band C gives very poor results with respect to the band X.

The results given by the Bayes Algorithm with two dimensions and using X and C band, are summarized in Table 2 (Frost filter). The mean probability of correct classification is equal to 87.8, as shown schematically in Fig. 6. Therefore, the performance of a classifier depends significantly on its dimensions. At the same time, some other data, as images in other bands or ground data, can be used to increase the probability of correct classification. As an example, by using the image in band IR shown in Fig. 5, and a three-dimensional Bayes algorithm, the probability of correct classification is equal to 91 (Fig. 6).

Two other algorithms have been considered as an alternative to the Bayes rule. The former, denoted in the following with D1, uses the Euclidean distance and the latter, denoted with D2, the city block distance. The mean probability of correct classification is shown schematically in Fig. 7. For the D1 algorithm, the probability of correct classification is equal to 81.97, while for the D2 algorithm is equal to 81.9. The Bayes classifier gives a probability equal to 87.8. Therefore, a reduction in performance is obtained; on the other hand, the computation time is significantly reduced.

#### REFERENCES

- /1/ R.A. Schowengerdt, "Techniques for Image Processing and Classification in Remote Sensing", Academic Press, London, 1983.
- /2/ F.T. Ulaby, R.Y. Li, K.S. Shanmugan, "Crop Classification Using Airborne Radar and Landsat Data", IEEE Trans. on Geoscience Electronics, pp. 42, 1982.
- /3/ J.W. Goodman, "Some Fundamental Properties of Speckle", J. Opt. Soc. Amer., pp. 1145-1150, 1976.
- /4/ J.S. Lee, "Digital Image Enhancement and Noise Filtering by Use of Local Statistics", IEEE Trans. on Pattern Anal. Machine Intell., pp. 165-168, 1980.
- /5/ V.S. Frost, J.A. Stiles, K.S. Shanmugan, J.C. Holtzman, S.A. Smith, "An Adaptive Filter for Smoothing Noisy Radar Images", Proc. of IEEE, pp. 133-135, 1981.
- /6/ V.S. Frost, J.A. Stiles, K.S. Shanmugan, J.C. Holtzman, S.A. Smith, "A Model for Radar Images and Its Application to Adaptive Digital Filtering", IEEE Trans. on Pattern Anal. Machine Intell., pp. 157-166, 1982.

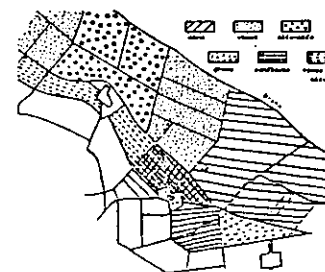


Fig. 1.



Fig. 2



Fig. 3

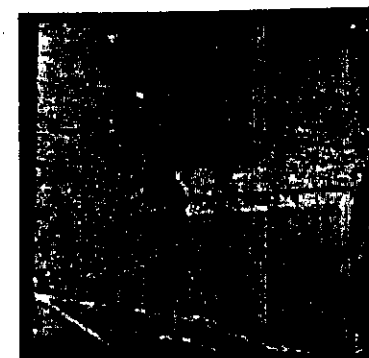


Fig. 4



Fig.5

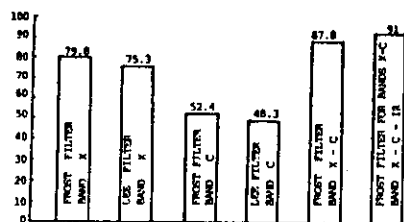


Fig.6

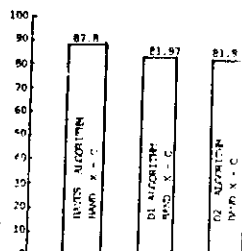


Fig.7

Crops	Original image		Image filtered with Lee Filter		Image filtered with Frost filter	
	Mean	Variance	Mean	Variance	Mean	Variance
Wheat	43.8	355	43.4	102	45.4	95
Dried Corn	35.7	285	34.4	110	37.2	85
Irrigated Corn	18.2	172	15.5	121	15.4	92
Soya-soya	54.8	473	48.0	271	58.3	136

Table 1

Crops	Probability of correct classification (%)			
	Wheat	Dried Corn	Irrigated Corn	Soya-soya
Wheat	87.6	12.0	0.2	0.2
Dried Corn	1.8	88.8	11.5	0
Irrigated Corn	0.8	12.1	87.1	0
Soya-soya	0	4.5	0	94.5

Table 2

V. CAPPELLINI, R. CARLA', V.M. SACCO, P. BENI, R. CAPPADONA  
Istituto di Ricerca sulle Onde Elettromagnetiche IROE-CNR  
Firenze, Italy

# A COST-EFFECTIVE NOAA SATELLITE IMAGE RECEIVING AND PROCESSING SYSTEM FOR DEVELOPING COUNTRIES

## ABSTRACT

The use of informations from meteorological satellites is today extended not only to weather analysis and forecasting but also to different application fields as oceanography, hydrology and agricultural studies. Applications in agriculture, land use, crop assessment and similar are very useful, mainly when referred to the developing countries of the world.

The availability of receiving & processing facilities which are simple to use, cost-effective and transportable is a very important tool for the development of those countries. For these purposes a receiving & processing station has been designed and realized at the IROE Institute to receive APT images from NOAA polar orbiting satellites.

In this paper a description of the station is reviewed in detail together with the operational performances. The station is easily transportable and it allows the receiving and the digital recording of many images in sequence without, practically, any operator intervention.

## 1. INTRODUCTION

The NOAA series of meteorological satellites transmits images of Earth surface in both digital HRPT (High Resolution Picture Transmission) and analogical APT (Automatic Picture Transmission) formats. Digital format data have a better resolution, but the APT protocol is more easily accessible and therefore less expensive than the digital one (1). The HRPT resolution is 1.1 km at the subsatellite point (nadir) and gets about five times worse at the end of the scan line because of the Earth curvature. An on-board digital processor (MIRP) removes these distortions and it gives an image with a nominal spatial resolution of about 4 km along each line. The processed image is transmitted using the APT format. Table 1 summarizes the APT signal characteristics.

Carrier frequency	137.50 MHz 137.62 MHz
Carrier polarization	right circular (RHCP)
Carrier modulation	analogic FM
Carrier deviation	+/- 17 KHz
EIRP (63° from nadir)	37.2 dBm nominal
Antenna gain	-0.5 dBi (63° from nadir)
Transm./antenna atten.	2.4 dB
Transmitter power	37.0 dBm min.
Subcarrier frequency	2.4 KHz DSB
Subcarrier modulation	analogic AM
Line frequency	120 per minute
Line synchronization	7 pulses at 1040 pps. (50% duty cycle ch. A) 7 pulses at 882 pps. (60% duty cycle ch. B)
Spatial resolution	4 km

Table 1 - NOAA/APT signal characteristics

RIENA, Space Meeting Proceedings, Rome 1987

In spite of the lower resolution the easiness of the reception makes the analogical data very interesting for many applications. It has been proved that the APT data offer good-quality quantitative measurements for application fields as oceanography, hydrology and agricultural studies (2). These considerations make very interesting the design of a NOAA/APT receiving station which is cost-effective, easily transportable and easy to use also for a non-experienced operator. Next sections describe the receiving & processing station design and realized at the IROE Institute.

## 2. STATION STRUCTURE

A block diagram of the developed IROE receiving system is shown in Fig. 1. The RF signal is received by an omnidirectional circular polarization antenna. The RF low-level noise preamplifier is just after the antenna. Then a telemetry VHF receiver realize a first down-conversion with an external generator as Local Oscillator (LO) and a second down-conversion with an internal LO. The receiver performs also the frequency demodulation of the signal. The resulting 2.4 KHz AM modulated subcarrier is the input of an APT demodulator realized at the IROE Institute. Finally the signal is digitally converted and stored on magnetic tapes. The images can be also displayed on-line on a TV monitor. Some characteristics of the receiving system components are described in detail.

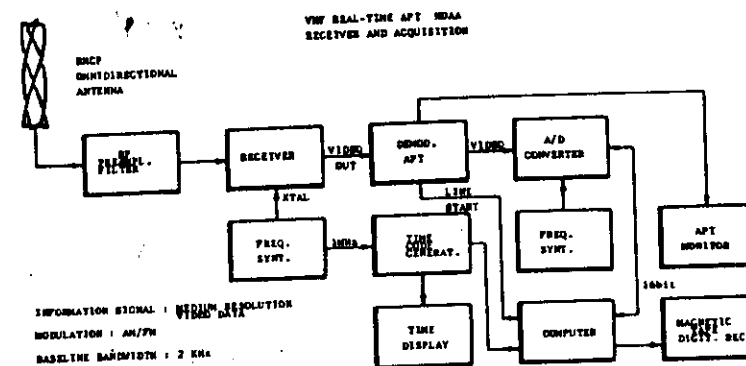


Fig. 1. Block diagram of the IROE receiving station

RIENA, Space Meeting Proceedings, Rome 1987

#### - Antenna

The RF ground power level of the satellite signal allows to use omnidirectional antennas with low-level gain and without satellite tracking. So an helicoidal antenna has been designed and realized to receive NOAA/APT signals with a right circular polarization (3). The lobe width is about  $160^\circ$  ( $\sim 3$  dB points) with a maximum gain of about 3 dBi at the zenith.

The antenna should be placed in a free horizon place, or as high as possible in urban areas, in order to minimize local reflections. The antenna is shown in Fig. 2.

#### - Antenna RF preamplifier

The antenna preamplifier is composed by two RF stages and a band-pass filter. The main characteristics are:

Frequency band	135.5 - 138.5 MHz
Gain	25 dB min.
Noise figure	4.0 dB max.
I/O impedance	50 $\Omega$ nom.

#### - Receiver

A telemetry receiver is used to receive the VHF signals with a double down-conversion. The receiver used is a Nems Clarke mod. R-1037F. For the APT 137.5 or 137.62 channels the configuration is the following:

RF Head : Nems Clarke mod. RFT-100A

Frequency band	135 - 155 MHz
Gain	30 dB
Noise figure	4.5 dB
Image rejection	>60 dB
IF rejection	>80 dB
First LO (external)	167.50 - 167.62 MHz

Band pass filter & IF Demodulator : Nems Clarke mod. PLD-105A (FM)

Filter frequency	10.035 MHz
" bandwidth	50 KHz ( $\pm 10\%$ at -3 dB points)
Demod. type	Phase lock
" distortion	2% max.
" sup. cut fr.	12.5 KHz $\pm 20\%$

The receiver works in Automatic Gain Control (AGC)

#### - Video signal demodulator (4)

This designed device performs the demodulation of the receiver output. It is a video signal AM modulated on a 2400 Hz subcarrier. The main components (in sequence) of the demodulator are:

Low-pass filter freq.	4000 Hz
High-pass "	700 Hz
Phase shift network	
Double balanced mod.	
Final low-pass filter	2000 Hz

The output is the modulating signal (0 - 1700 Hz).

With a suitable circuitry the Start of Frame (SOF) signal is de-

tected and a flag allows the computer to begin correctly the acquisition.

#### - A/D Conversion

All the system is computer controlled in order to perform the A/D conversion, the image synchronization and finally the digital recording on magnetic tapes.

An A/D converter HP mod. 5610A (resolution 10 bit) is used together with a parallel interface between the A/D converter and the computer.

#### - Computer and peripherals

The central computer unit is a mini-computer HP 1000 (16 bit word) with some typical peripherals as monitor, printer, disk, magnetic tape unit etc. Some other types of mini or personal computer could be used in order to drive the receiving system.

### 3. OPERATIONAL PERFORMANCES

The operational performances of the system include, as already mentioned, the reception and the data processing of the NOAA/APT images together with the A/D conversion and the digital recording. A suitable software package has been implemented on the computer (normally in assembler language) to perform all the preceding actions. Practically the operator has to define only the acquisition start times. These values of time can be computed by a suitable off-line routine which knows both the geographical location of the station and the orbital characteristics of the spacecraft. More complex processing operations can be performed off-line on the stored images using a VDS-701 pictorial memory unit connected to the computer. The developed software package includes the following processing:

- Image calibration (5)
- Digital filtering to enhance the received images or to reduce noise effects (6)
- Digital comparison and correlation among images received from different bands (multispectral analysis) or at different hours (multitemporal analysis)
- Pattern Recognition techniques to extract and recognize Earth regions having specific interesting properties.

Fig. 3a shows a NOAA/APT image in the near-infrared band (0.725-1.1  $\mu$ m), received on May 13, 1985 at 13.27 GMT. Fig. 3b represents the corresponding thermal infrared band image. Fig. 4b shows the result obtained processing the original image (Fig. 4a) with a suitable "extremal median filtering" technique, in order to remove unwanted noise spikes.

### 4. CONCLUSIONS

A station for the NOAA/APT image reception, acquisition and processing is described. Among the other characteristics of the station the low-cost, the transportability, the automation of the procedures (which are completely computer controlled) and the easiness of the use have been underlined.

These and other performances, as many post-processing features, allow to use the station in many application fields and not only in meteorology. For example the use of such stations could be a very important tool in agronomic studies, particularly in the developing countries.

#### REFERENCES

- 1 Schwalb A., "Modified version of the TIROS-N/NOAA A-G satellite series (NOAA E-J). Advanced TIROS-N (ATN)". NOAA Tech. Mem. NESS 116, Washington D.C., Feb. 1982
- 2 Wannamaker B., "An evaluation of digitized APT data from the TIROS-N/NOAA -A,-J series of meteorological satellites". Int. Journal of Remote Sensing, 1984, V.5, N1, pp. 133-144
- 3 Beni P., Cappadona R., "Un'antenna omnidirezionale a polarizzazione circolare per la ricezione di segnali da satelliti in banda VHF". Tech. Rep. IROE-CNR, Firenze, Oct. 1985
- 4 Beni P., Carla' R., Venturi V., "Descrizione del sistema di ricezione, acquisizione e di elaborazione dati APT da satelliti TIROS-N/NOAA". Tech Rep. IROE-CNR, Firenze, March 1986
- 5 Schwalb A., "The TIROS-N/NOAA A-G Satellite Series". Tech. mem. NESS-95, Washington D.C., Reprinted 1982
- 6 Carla' R., Sacco V.M., Baronti S., "Digital techniques for noise reduction in APT satellite images". Proc. of Int. Conf. IGARSS '86, Zurich, Sept. 1986, pp.995-1000

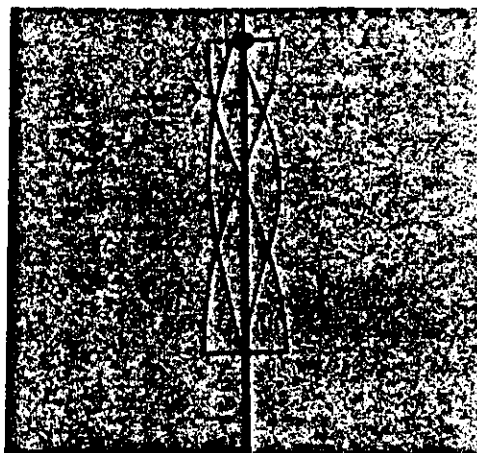


Fig. 2 Omnidirectional VHF antenna

RIENA, Space Meeting Proceedings, Rome 1987

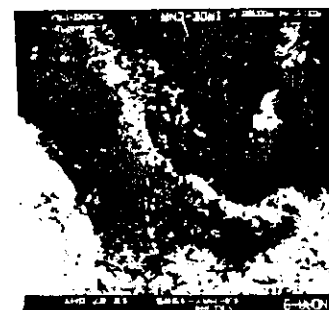


Fig. 3a Near infrared band image received on May, 13, 1985



Fig. 3b Thermal infrared band image as Fig. 3a

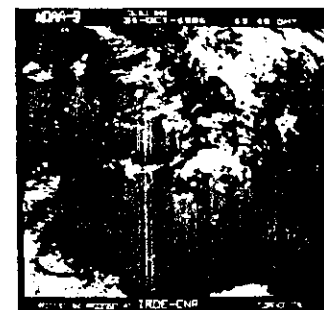


Fig. 4a Near infrared band original image

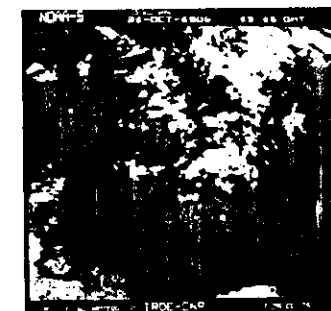


Fig. 4b Processing output of the image of Fig. 4a

RIENA, Space Meeting Proceedings, Rome 1987